Available online at www.sciencedirect.com

ScienceDirect

Procedia Structural Integrity 57 (2024) 375–385

Structural Integrity Procedia

www.elsevier.com/locate/procedia

Fatigue Design 2023 (FatDes 2023)

# Exploration of the orientational-dependent fatigue response of triply periodic minimal surface cellular structures: A numerical study

Sudeep K. Sahoo[a,*], Nicolas Saintier[a], Yves Chemisky[a]

[a]*Université de Bordeaux, Laboratoire I2M, Arts et métiers ParisTech - CNRS UMR 5295, F-33400 Talence, France*

**Abstract**

Recently, Triply Periodic Minimal Surface (TPMS)-based lattices have received significant attraction in structural applications across a variety of engineering sectors, including automobile, aerospace, and biomedical, owing to their improved mechanical properties and lightweight potential. The mechanical characteristics of these lattices are intrinsically linked to the design-related topological descriptors that include the spatial arrangement of their topological cell wall, geometrical sizes, and relative density. In practical applications, however, these structures are often exposed to fluctuating loads that can induce depreciation of their mechanical properties and eventually fatigue failure. Therefore, it is crucial to conduct a comprehensive analysis of their orientational-dependent fatigue response and explore the structure-property correlation under fatigue subjected to various loading conditions. To address this challenge, a novel numerical framework based on the Finite Element Method has been proposed and employed to investigate the fatigue strength of TPMS lattices, specific to uniaxial loading conditions. The stress-based Crossland criterion has been adopted as the fatigue criterion, and the fatigue strength of the considered volume is computed using a fatigue indicator parameter (FIP). The developed framework is undertaken to examine the performance of two widely studied sheet-based TPMS-lattices, namely Schoen Gyroid, and Schwarz Primitive. Besides, the approach permitted to demonstrate the influence of localized material distribution and loading direction towards the evaluation of fatigue strength and structural efficiency. It is observed that among the proposed lattices, Schoen Gyroid is shown to exhibit better fatigue properties in accordance with the existing literature studies. The outcome of these case studies suggests that the proposed numerical framework offers a promising solution for solving topology optimization problems involving lattices, wherein not only the selection of the lattice but also their preferred orientation can be taken into account as design variables.



*Keywords:* Triply Periodic Minimal Surface; Finite Element Method; Crossland Criterion; Fatigue Response; Topology Optimization.

## 1. Introduction

The exploration of light-weighting the structural components continues to be an active and dynamic field of research and development, spanning multiple sectors. In particular, the automotive and aerospace industries consider

* Corresponding author.
*E-mail address:* sudeep-kumar.sahoo@ensam.eu


10.1016/j.prostr.2024.03.040

light-weighting as a pivotal strategy for enhancing fuel efficiency and mitigating environmental challenges by reducing emissions. Apparently, this has sparked a significant surge in interest and research efforts toward finding innovative solutions, such as lightweight materials and structures, that offer promising solutions for leveraging these benefits. Parallel to these developments, the rapid advancements in additive manufacturing (AM) technology have attracted considerable interest among researchers, particularly in the realm of fabricating lightweight lattice structures. These structures exhibit complex geometries and a repetitive arrangement of unit cells, showcasing a diverse spectrum of adjustable multifunctional properties that are intricately influenced by their distinctive topology (Lu et al. (2022); Yu et al. (2018)). By carefully designing the unit cell topology, lattice structures can be tailored to demonstrate desirable properties, such as high strength-to-weight ratios, low densities, high energy absorption capabilities, high surface area-to-volume ratio, and tunable porosities derived from their engineered micro-architecture (Maconachie et al. (2019); Poltue et al. (2021); Refai et al. (2020b); Sharma and Hiremath (2020)).

**Nomenclature**

| | |
|---|---|
| TPMS | Triply Periodic Minimal Surfaces |
| $X, Y, Z$ | Cartesian Coordinate System |
| $n$ & $L$ | number and length of the unit cell, respectively |
| $c$ | level-set parameter |
| $\bar{\rho}$ | Relative density of the lattice structure |
| $\bar{\sigma}_{ij}$ | Equivalent Stress field (Second-rank tensor) |
| $\bar{\varepsilon}_{kl}$ | Equivalent Strain (Second-rank tensor) |
| $\bar{C}_{ijkl}$ | Homogenized effective stiffness matrix (Fourth-order tensor) |
| RVE | Representative Volume Element |
| $V_{RVE}$ | Overall volume of the RVE |
| $v$ | Effective (or the real) volume of the lattice cell |
| $\sigma_{eq.\ Cross}$ | Equivalent Crossland Stress |
| $J_{2,a}$ | $2^{nd}$ invariant of deviatoric stress amplitude |
| $\sigma_{H,\max}$ | Maximum Hydrostatic Stress |
| $\alpha$ & $\beta$ | Crossland Criterion parameters |
| $FIP$ | Fatigue Indicator Parameter |
| $C_s$ | Coefficient of Security |
| $E_s$ | Elastic Modulus |
| $\nu_s$ | Poisson's ratio |
| $R$ | Fully reversed loading condition ($R = -1$) |
| $A_r$ | Anisotropic Ratio |

Depending upon the topological arrangement, the unit cells of the lattice structures can be broadly categorized into two main types: strut-based lattices and sheet-based lattices. Strut-based lattices are characterized by interconnected struts forming the unit cell at the nodes, while sheet-based lattices consist of thin walls composing the unit cell. Within the realm of sheet-based lattices, Triply Periodic Minimal Surface (TPMS) structures have garnered significant attention in recent years. TPMS structures are characterized by non-self-intersecting surfaces with zero mean curvature, which can be described mathematically using specific equations (Al-Ketan et al. (2019); Bobbert et al. (2017); Chatzigeorgiou et al. (2022); Refai et al. (2020a)). Furthermore, the absence of nodes and discontinuities in their curvature leads to decreased stress concentration, thereby improving their mechanical performance. Understanding the fatigue response of lattice structures, on the other hand, is crucial in real-time scenarios because the structural parts constructed by tessellating these elementary cells are exposed to unprecedented cyclic loading conditions which impact their structural performance. External parameters such as vibrations, fluctuating loads, rotational or reciprocating motion, thermal cycling, etc., or a combination of these parameters often contribute towards these cyclic stresses. As a consequence, stress concentration occurs in certain sections, resulting in the degradation of mechanical properties and an unforeseen risk of failure (Kelly et al. (2019); Molavitabrizi et al. (2022)). In light of this, precise prediction and

characterization of the fatigue performance of these cellular structures are essential for a comprehensive understanding of the issues involved, especially when dealing with the interconnected complicated cell wall morphology.

A comprehensive review of fatigue studies on lattice structures pointed out that the fatigue properties of cellular solids, including their mechanical properties, are mainly governed by several key aspects: (i) the mechanical properties of the bulk material, (ii) relative density, (iii) cell geometry, and (iv) material distribution within the structure, which determines the shape of cell walls or struts (Ahmadi et al. (2015); Cutolo et al. (2020); Downing et al. (2021); Maskery et al. (2015); Yavari et al. (2015)). Pursuing an experimental strategy to examine the influence of these factors on the fatigue properties of lattice structures can be a time-consuming and resource-intensive endeavor since a large number of samples are required for fatigue testing, which incurs additional expenses. Alternatively, the computational method offers a robust and efficient approach to accelerate the process by simulating experimental conditions. In this regard, several numerical models (Molavitabrizi et al. (2022); Peng et al. (2021); Peng et al. (2022); Refai et al. (2020a)) have been proposed to predict the fatigue behavior. However, a research gap still remains for the development of a numerical framework that could effectively predict the orientational-dependent fatigue characteristics.

Based on this perspective, the present investigation is undertaken with two main objectives. Firstly, a numerical framework is proposed to assess the fatigue behavior of lattice structures under uniaxial loading conditions. This approach utilizes the local stress-based Crossland criterion and computes the fatigue strength of the analyzed volume using a fatigue indicator parameter ($FIP$). Secondly, a suitable technique is proposed to visually demonstrate the computed mechanical response in a three-dimensional spatial representation. This representation aids in exploring the anisotropic behavior and orientation dependence of the lattice properties under investigation. The reliability of the proposed approach was tested critically by applying it to two sheet-based TPMS lattice structures, namely Schoen Gyroid and Schwarz Primitive. Consequently, the developed numerical framework enables the identification of critical sections within these lattice structures corresponding to the high symmetry directions of the cubic crystal, specifically [001], [110], and [111] loading directions. The main finding of this proposed framework serves as a valuable tool for effectively directing the design and optimization process to tailor the material's mechanical properties to meet specific application requirements, thereby ensuring the durability and safety of components and structures.

## 2. Numerical Methodology

### 2.1. Modelling the TPMS Cellular structures: Design and Generation

In this section, the design strategy to model TPMS-based lattice structures is obtained using the level-set trigonometrical equations (Chatzigeorgiou et al. (2022); Krishnan et al. (2022)), defined as:

$$f_i(x, y, z) = c \tag{1}$$

where, $x = 2\pi nX/L$, $y = 2\pi nY/L$, and $z = 2\pi nZ/L$. Here, the variables $X$, $Y$, and $Z$ represent the cartesian coordinate system, while $n$ and $L$ denote the number and length of the unit cell, respectively. The parameter '$c$' in Eq. 1 represents the level-set parameter, which determines the offset of the minimal surfaces, and controls the volume ratio between the two sub-spaces. Specifically, for the extensively studied lattice structures, namely the Schoen Gyroid and the Schwarz Primitive, the corresponding level-set functions are expressed as follows:

$$(a)\ Schoen\ Gyroid: f_G(x, y, z) = \cos(x) \cdot \sin(y) + \cos(y) \cdot \sin(z) + \cos(z) \cdot \sin(x) \tag{2}$$

$$(b)\ Schwarz\ Primitive: f_P(x, y, z) = \cos(x) + \cos(y) + \cos(z) \tag{3}$$

By tuning the '$c$' parameter, different desired density levels for both the Schoen Gyroid and the Schwarz Primitive lattice structures are generated. The resultant lattice structures with varying relative density levels are modeled using an in-house open-source software microgen (https://github.com/3MAH/microgen) and are shown in Fig. 1(a),(b). In this context, the relative density (or volume fraction) denoted by $\bar{\rho}$ for a lattice structure is defined as:

$$\bar{\rho} = \frac{\rho_{Latt}}{\rho_S} \tag{4}$$

where, $\rho_{Latt}$ and $\rho_S$ denote the densities of the lattice structure and the constituent base material, respectively. The parameter $\bar{\rho}$ ranges from 0 to 1, with 1 indicating a fully solid structure. Both these lattice structures are well-known for their unique geometries and potential applications in various structural domains.

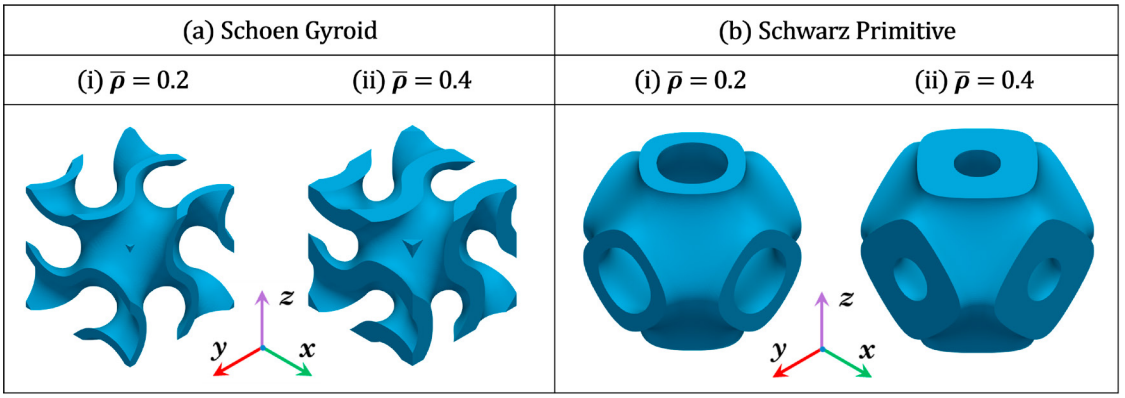


Fig. 1: Sheet-based Triply Periodic Minimal Surface (TPMS) lattice structures with relative density levels of 0.2 and 0.4 for: (a) Schoen Gyroid and (b) Schwarz Primitive.

### 2.2. Computational Homogenization Framework

From the geometrical perspective of these lattice structures, it is evident that the presented lattices possess cubic symmetry and may exhibit distinct topological-mechanical property relationships as a result of different cell-wall topologies. In this aspect, it is crucial to establish a thorough understanding of the interaction between the macroscopic properties of architected cellular materials and the design parameters associated with the lattice cell, such as unit cell type and relative density. These relationships can be effectively determined using the numerical homogenization method to evaluate the effective mechanical properties, which relies on generalized Hooke's law. In this context, the TPMS unit cell (shown in Fig. 1) is selected as the representative volume element (RVE) and is treated as an equivalent homogeneous solid continuum whose mechanical response is described by a set of effective (or equivalent) material properties.

According to the generalized Hooke's law, the relationship between the equivalent stress field ($\bar{\sigma}_{ij}$) and the equivalent strain ($\bar{\varepsilon}_{kl}$) for the sheet-based TPMS can be expressed as:

$$\bar{\sigma}_{ij} = \bar{C}_{ijkl}\bar{\varepsilon}_{kl} \tag{5}$$

where, $\bar{\sigma}_{ij}$, $\bar{\varepsilon}_{kl}$, and the stiffness matrix ($\bar{C}_{ijkl}$) can be further defined as:

$$\begin{bmatrix} \sigma_{11} \\ \sigma_{22} \\ \sigma_{33} \\ \sigma_{23} \\ \sigma_{12} \\ \sigma_{13} \end{bmatrix} = \begin{bmatrix} C_{11} & C_{12} & C_{13} & C_{14} & C_{15} & C_{16} \\ & C_{22} & C_{23} & C_{24} & C_{25} & C_{26} \\ & & C_{33} & C_{34} & C_{35} & C_{36} \\ & sym & & C_{44} & C_{45} & C_{46} \\ & & & & C_{55} & C_{56} \\ & & & & & C_{66} \end{bmatrix} \begin{bmatrix} \varepsilon_{11} \\ \varepsilon_{22} \\ \varepsilon_{33} \\ 2\varepsilon_{23} \\ 2\varepsilon_{12} \\ 2\varepsilon_{13} \end{bmatrix} \tag{6}$$

Furthermore, due to the cubic symmetric nature of the presented sheet-based TPMS, the elastic constants in the stiffness matrix can be well represented by means of three independent constants as: $C_{11} = C_{22} = C_{33}$, $C_{12} = C_{13} = C_{23}$, $C_{44} = C_{55} = C_{66}$. The remaining constants in the matrix are set to zero. Based on these considerations, the stiffness matrix can be expressed in a simplified form:

$$\begin{bmatrix} \sigma_{11} \\ \sigma_{22} \\ \sigma_{33} \\ \sigma_{23} \\ \sigma_{12} \\ \sigma_{13} \end{bmatrix} = \begin{bmatrix} C_{11} & C_{12} & C_{12} & 0 & 0 & 0 \\ & C_{22} & C_{12} & 0 & 0 & 0 \\ & & C_{33} & 0 & 0 & 0 \\ & sym & & C_{44} & 0 & 0 \\ & & & & C_{55} & 0 \\ & & & & & C_{66} \end{bmatrix} \begin{bmatrix} \varepsilon_{11} \\ \varepsilon_{22} \\ \varepsilon_{33} \\ 2\varepsilon_{23} \\ 2\varepsilon_{12} \\ 2\varepsilon_{13} \end{bmatrix} \tag{7}$$

In order to evaluate the values of three unknown constants in the stiffness matrix (Eq. 7), two FEM analyses are required to be performed on the RVE: one for uniaxial and the other for shear strain. The strain conditions for these computations are as follows:

$$For\ uniaxial\ strain : \varepsilon_{kl} = \begin{bmatrix} 1 & 0 & 0 & 0 & 0 & 0 \end{bmatrix}^T \tag{8}$$

$$For\ shear\ strain : \varepsilon_{kl} = \begin{bmatrix} 0 & 0 & 0 & 1 & 0 & 0 \end{bmatrix}^T \tag{9}$$

It is worth noting that in the linear elastic model, the imposed strain value has no influence on the stiffness properties of the lattices. Hence, a unit value is adopted for simplicity. Eventually, the stiffness tensor $\bar{C}_{ij}$ can be established by calculating the average of the local fluctuation of the stress fields within the unit cell. The homogenized stress ($\bar{\sigma}_{ij}$) under such scenario is determined based on Hill's principle (Hill (1963)):

$$\bar{C}_{ij} = \bar{\sigma}_{ij} = \frac{1}{V_{RVE}} \int_v \bar{\sigma} dV \tag{10}$$

where, $\bar{\sigma}$ denotes the stress components of the stress tensors within the differential volume element $dV$, $V_{RVE}$ is the overall volume of the RVE, and $v$ is the effective (or the real) volume of the lattice cell.

### 2.3. Modelling the Multiaxial High-cycle Fatigue Criterion

As a fatigue criterion, the stress-based Crossland criterion (Crossland et al. (1956)) is adopted for evaluating the heterogeneity of the fatigue stress field. Mathematically, this criterion represents a linear combination of the maximum value of the hydrostatic stress over a cycle ($\sigma_{H,\max}$) and amplitude of the second invariant of the deviatoric tensor ($\sqrt{J_{2,a}}$) and is expressed as:

$$\sigma_{eq.\ Cross} = \sqrt{J_{2,a}} + \alpha \cdot \sigma_{H,\max} \leq \beta \tag{11}$$

Here, $\sigma_{eq.\ Cross}$ is the equivalent Crossland stress, whereas $\alpha$ and $\beta$ are two material parameters to be identified from the fatigue tests, measured for a given number of cycles under alternated tensile and shear stress conditions, respectively. The calculation of $\sqrt{J_{2,a}}$ is obtained by a double maximization over the whole loading cycle:

$$\sqrt{J_{2,a}}(M) = \frac{1}{2\sqrt{2}} \left( \max_{t_i \in T} \left\{ \max_{t_j \in T} \sqrt{\left[ \overline{\overline{S}}\,(t_i) - \overline{\overline{S}}\,(t_j) : \overline{\overline{S}}\,(t_i) - \overline{\overline{S}}\,(t_j) \right]} \right\} \right) \tag{12}$$

where, $\overline{\overline{S}}$ is the deviatoric part of the stress tensor, and the symbol ":" expresses the contracted double product. $t$ and $T$ are the time and the loading period, respectively. The maximum hydrostatic stress ($\sigma_{H,\max}$) over a cycle (shown in 11) is defined as:

$$\sigma_{H,\max} = \max_{t \in T} \left( \frac{1}{3} \sum_{k=1}^{3} \sigma_{kk} \right) \tag{13}$$

where, $\sigma_{kk}$ (k = 1, 2, 3) are the diagonal elements of the stress tensor.

Following the principles of the Crossland criterion (Eq. 11), the fatigue strength of the considered volume is evaluated using a fatigue indicator parameter ($FIP$) proposed by Vayssette et al. (2019), which is expressed as:

$$FIP_{max} = \sqrt{J_{2,a}} + \alpha \cdot \sigma_{H,\max}, \quad or, \quad FIP_{max} = \beta \tag{14}$$

The given expression (Eq. 14) facilitates the construction of the Crossland plot (also referred to as $\sqrt{J_{2,a}}$ versus $\sigma_{H,max}$ plot), as shown in Fig. 2, and the dashed line in the plot represents the line of the equation:

$$\sqrt{J_{2,a}} + \alpha \cdot \sigma_{H,\max} = \beta \tag{15}$$

which governs the fatigue limit.

The fatigue strength of a specific volume is considered to have been attained when the representative point ($M$) in Fig. 2 reaches the material threshold line. This point of intersection is referred to as the coefficient of security ($C_s$),

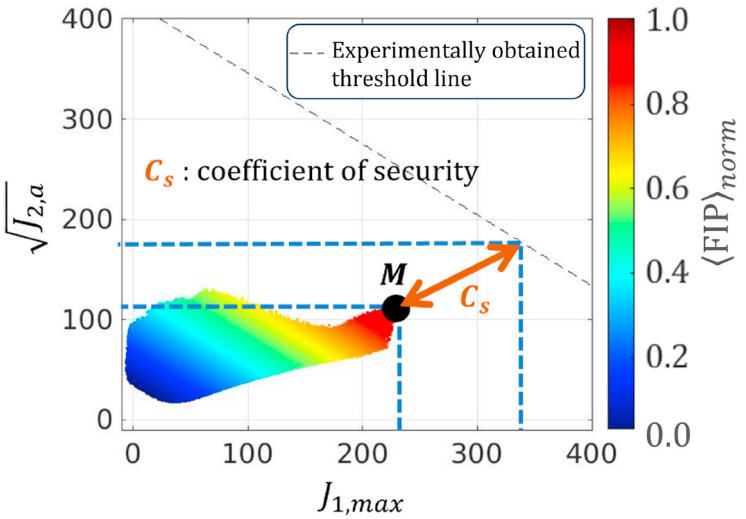


Fig. 2: Crossland plot showing the representative point (M) and the material threshold line along with the coefficient of security.

which is proportional to the distance between the representative point ($M$) and the material threshold line (as shown in Fig. 2. Here, the representative point ($M$) denotes the coordinate point where the value of $FIP$ is maximum.

By combining Eqs. 11, 14 and solving them, the following expression for the coefficient of security ($C_s$) can be obtained:

$$C_s(M) = \frac{\beta}{FIP_{max}}, \quad or, \quad C_s(M) = \frac{\beta}{\sqrt{J_{2,a}} + \alpha \cdot \sigma_{H,\max}} \tag{16}$$

Now, considering a unit safety factor (SF = 1), that is, when the $FIP_{max}$ is equal to the Crossland parameter ($\beta$) for a given macroscopic loading, the fatigue strength ($\bar{\sigma}_f$) is evaluated as:

$$\bar{\sigma}_f = \frac{\bar{\sigma}_m \times \beta}{FIP_{max}} \tag{17}$$

where $\bar{\sigma}_m$ is the amplitude of the arbitrary initial applied load. In the present context, this will be referred to as *"macroscopic fatigue strength"*.

In addition, the present study also aims to investigate the influence of orientation on the fatigue strength of the presented TPMS unit cells. To accomplish this, the stress tensor, a fundamental concept in mechanics, is employed to describe the stress state of the material corresponding to a specific orientation. This assessment can be readily accomplished by maintaining the lattice cell constant and employing the mechanics of stress tensor coordinate transformation, which allows for the conversion of the initial reference coordinate system to the new coordinate system. Such a procedure enables us to determine the resultant stress tensor components generated as a result of these transformations.

### *2.4. Simulation Procedure*

In the present investigation, the finite element analysis is accomplished using the Zebulon implicit solver (Z-Set), a commercial finite element software, to compute the fatigue as well as the anisotropic response of TPMS-based lattice structures. The FEA mesh was constructed using Second-order tetrahedral elements (C3D10) because of its geometric flexibility and ability to handle complex geometries, thus allowing for a more precise analysis of the deformation response. To ensure computational accuracy and adequate geometric conformance, a mesh convergence analysis was performed. An element size of 0.06 mm was selected, as it provided the necessary computational precision and geometric fidelity. Concerning the base material behavior, linear elastic, perfect plastic, and rate-independent are assumed. Titanium alloy (Ti-6Al-4V) is chosen as the solid base material, with the following material properties:

Elastic modulus ($E_s$) = 110 GPa, and Poisson's ratio ($\nu_s$) = 0.3. The fatigue coefficients for the same alloy, that is, $\alpha$ = 0.707 and $\beta$ = 416.7 MPa were adopted from the experimental work of Vayssette et al. (2019). The fatigue simulations in this study are conducted under uniaxial loading conditions with fully reversed loading, for load ratio ($R$) = -1. The obtained results for the fatigue strength are graphically represented using a spherical coordinate system; the details of which can be found in Nordmann et al. (2018).

## 3. Results and Discussion

### *3.1. Assessing the Fatigue Strength*

Fig. 3 presents the three-dimensional spatial representation of fatigue strength of the examined sheet-based TPMS lattice at relative density levels of 0.2 and 0.4, under uniaxial loading conditions. To evaluate the fatigue strength, the numerical framework (as mentioned in subsection 2.3) based on the stress-based Crossland criterion (Crossland et al. (1956)) is being adopted. It is important to note that, for all considered lattice structures, the fatigue responses are observed at the same stress level. Here, the primary focus is to shed light on the impact of the intriguing topological sheet arrangements and anisotropic characteristics of TPMS structures on their fatigue response when subjected to different loading orientations. The plot displays variations in fatigue strength across the lattice structure, as shown in Fig. 3, with different colors demonstrating the range of fatigue strength values reflected in the color scale bar. Ideally, this three-dimensional shape function is typically characterized by a perfect sphere to represent isotropic material behavior, demonstrating consistent mechanical properties in all directions. However, any deviation from this shape indicates the level of anisotropy, highlighting the directional dependence of these properties in terms of strong and weak directions.

It can be observed that the Schoen Gyroid structure demonstrates minimal variation in the fatigue strength irrespective of the loading direction, with deviations within the range of ±5% from the mean value. While the primitive structure displayed a significant variation in fatigue strength depending on the loading direction relative to the sheet orientation. The highest fatigue strength is observed along the diagonal direction and the lowest fatigue strength along the axial direction, which corresponds to the [111] and [001] loading directions, respectively. This disparity in fatigue strength between the Schoen Gyroid and Schwarz Primitive is primarily attributed to the unique alignment of the cell wall arrangement within these structures with respect to the different loading orientations.

#### *3.1.1. Influence of cell wall topology*

Concerning the topological cell wall arrangement, the Schoen Gyroid demonstrates an efficient configuration of cell walls that optimizes load distribution within the structure. The complex spiraling interconnected sheets form a highly efficient network, facilitating the distribution and transfer of loads throughout the structure. This unique micro-architecture enables a homogeneous fatigue response along various orientations, as the load is evenly dispersed and shared across the interconnected network of cell walls. Consequently, the gyroid structure exhibits a more isotropic behavior, meaning its mechanical properties are relatively consistent regardless of the direction of applied stress. Indeed, previous studies (Bobbert et al. (2017); Yang et al. (2019)) on the deformation behavior of Schoen Gyroid have also pointed out similar responses.

The micro-architecture of the Schwarz Primitive structure, on the other hand, is primarily driven by more regular and straight sheet configurations, and it lacks the complex spiral network of support found in the gyroid structure. As a consequence of such a design, the effective load transfer between neighboring sheets is limited, resulting in more heterogeneous stress distribution. This shows that the configuration of cell walls is important in aiding load transmission and the structure's ability to resist deformation, influencing stress distribution across neighboring sheets. Besides, it can be observed from Fig. 3, that increase in the relative density of the lattice structures resulted in higher fatigue strength for both structures. This is based on the fact that higher relative density typically leads to increased stiffness and resistance to deformation.

### *3.2. Anisotropic response*

A better understanding of the anisotropic behavior of the lattice structures can be further quantified using the Zener anisotropy index. This index, introduced by Zener and Siegel (1949), quantifies the degree of anisotropy exhibited

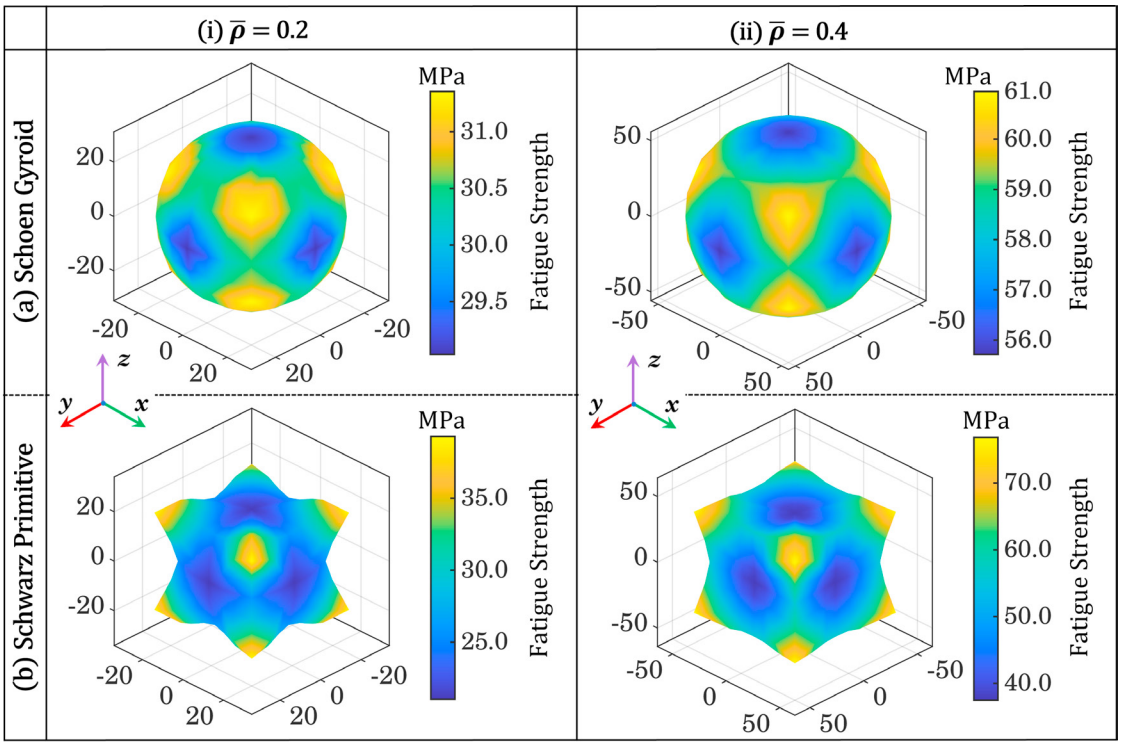


Fig. 3: Three-dimensional spatial representation of the fatigue strength at specified relative density levels for (a) Schoen Gyroid, and (b) Schwarz Primitive.

by the material, also referred to as anisotropic ratio ($A_r$). It is defined as the ratio of the shear modulus of the cubic lattice, $C_{44}$, to that of an isotropic material under the same stretching, $(C_{11} - C_{12}/2)$ and reads as:

$$A_r = \frac{2C_{44}}{C_{11} - C_{12}} \tag{18}$$

Here, $C_{44}$ represents the resistance to shear stress applied across the (100) plane in the [010] direction, and $(C_{11} - C_{12}/2)$ is the resistance to shear stress applied across the (110) plane in the direction $[1\bar{1}0]$ (Abueidda et al. (2016)). According to Eq. 18, when $A_r = 1$ the lattice structure is considered isotropic, indicating that the material exhibits the same mechanical properties in all directions. Conversely, any deviation from $A_r = 1$ signifies the presence and extent of anisotropy induced by the specific topological arrangement of the lattice structure.

Fig. 4 presents the anisotropic behavior of the lattice structures as a function of relative density. The plot reveals that the Zener ratio for the Schoen Gyroid demonstrates a response close to isotropy ($A_r \approx 1$), and remains relatively constant even with increasing relative density up to 0.5. In contrast, the Schwarz Primitive, despite belonging to the same family of sheet-based TPMS, displays a pronounced anisotropic behavior, as indicated by its significant deviation from isotropy. However, as the relative density increases, the anisotropy of the Schwarz Primitive gradually decreases. This is primarily attributed to the increased thickness of the cell wall, which transforms the porous structures into solid ones, leading to a loss of the beneficial porous features. The contrasting anisotropic responses between the two lattice structures, Schoen Gyroid and Schwarz Primitive, emphasize the influence of their geometric configurations on mechanical performance, particularly in relation to the micro-architecture of the cell wall.

### *3.3. Identifying the critical sections and distribution of the Crossland Stress distribution pattern*

To gain deeper insights into the deformation mechanisms of lattice structures under uniaxial loading conditions, the Crossland stress field distribution is investigated for two examined geometries at relative density levels of 0.2 and 0.4. The study focuses on specific loading orientations, namely [001], [110], and [111] and the results are presented in Fig.

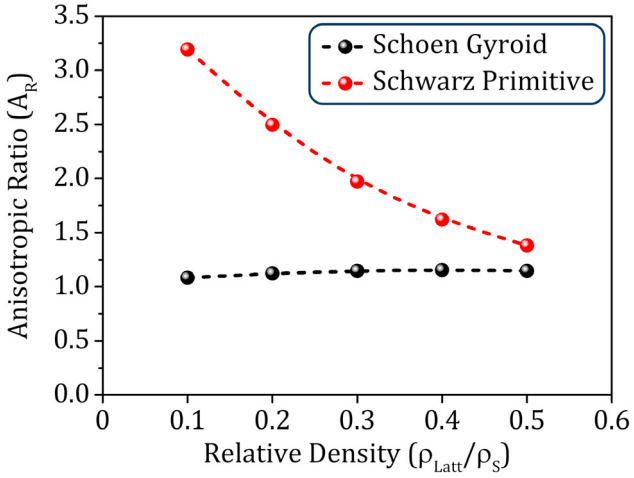


Fig. 4: Variation of anisotropic ratio ($A_r$) as a function of relative density ($\bar{\rho}$) for the Schoen Gyroid and Schwarz Primitive.

5. The figures reveal that distinct regions within the lattice structures experience varying stress levels depending on the loading orientation relative to the structure's axes. These critical regions are of significant interest as they indicate areas of high stress where the probability of material failure is more likely to occur. In addition, it is evident that the highest stressed regions align consistently with the loading orientations.

By analyzing the sections of the Schoen Gyroid (Fig. 5a), it becomes apparent that stress is redistributed homogeneously among all the branches of the interconnected sheet network irrespective of the loading directions. However, the branches aligned relative to the loading direction experience the highest stress levels as compared to the others. Such arrangement of topological call wall offers a plausible explanation for the Schoen Gyroid's isotropic behavior in terms of mechanical performance and superior fatigue resistance, particularly when subjected to heterogeneous loading conditions.

In contrast, the Schwarz Primitive (Fig. 5b) structure exhibits high anisotropy. When subjected to loading orientations along [001], and [110], specific locations along the loading direction experience concentrated regions of high stress. While along [111] direction, the distribution of the cell walls is preferentially aligned with a greater volume of the lattice structure to resist the deformation, thereby providing higher fatigue strength. However, due to the increased anisotropy of the lattice structure, Schwarz Primitive structures are more prone to stress concentration and cracking when exposed to heterogeneous loading conditions.

## 4. Conclusions

To conclude, the numerical framework proposed in this study provides an efficient and effective method for evaluating the orientational-dependent fatigue response of lattice structures. Our results emphasize the importance of geometry, spatial arrangement of cell wall topology, cell wall curvature, and relative density in regulating the mechanical behavior of lattice systems. The key findings are highlighted as follows:

(1) The Schoen Gyroid lattice demonstrated better fatigue qualities, which is consistent with prior findings in the literature. This enhanced performance is due to the helical structure of its cell walls, which allows for homogeneous load distribution over the whole cell volume independent of the loading direction.

(2) The Schwarz Primitive lattice presents more localized stress fields for specific loading directions, demonstrating its sensitivity to loading direction and thus influencing the fatigue response.

In summary, our proposed methodology provides useful insights that lead to a better understanding of these materials' overall mechanical characteristics for the design and optimization of lattice structures in a variety of engineering applications.

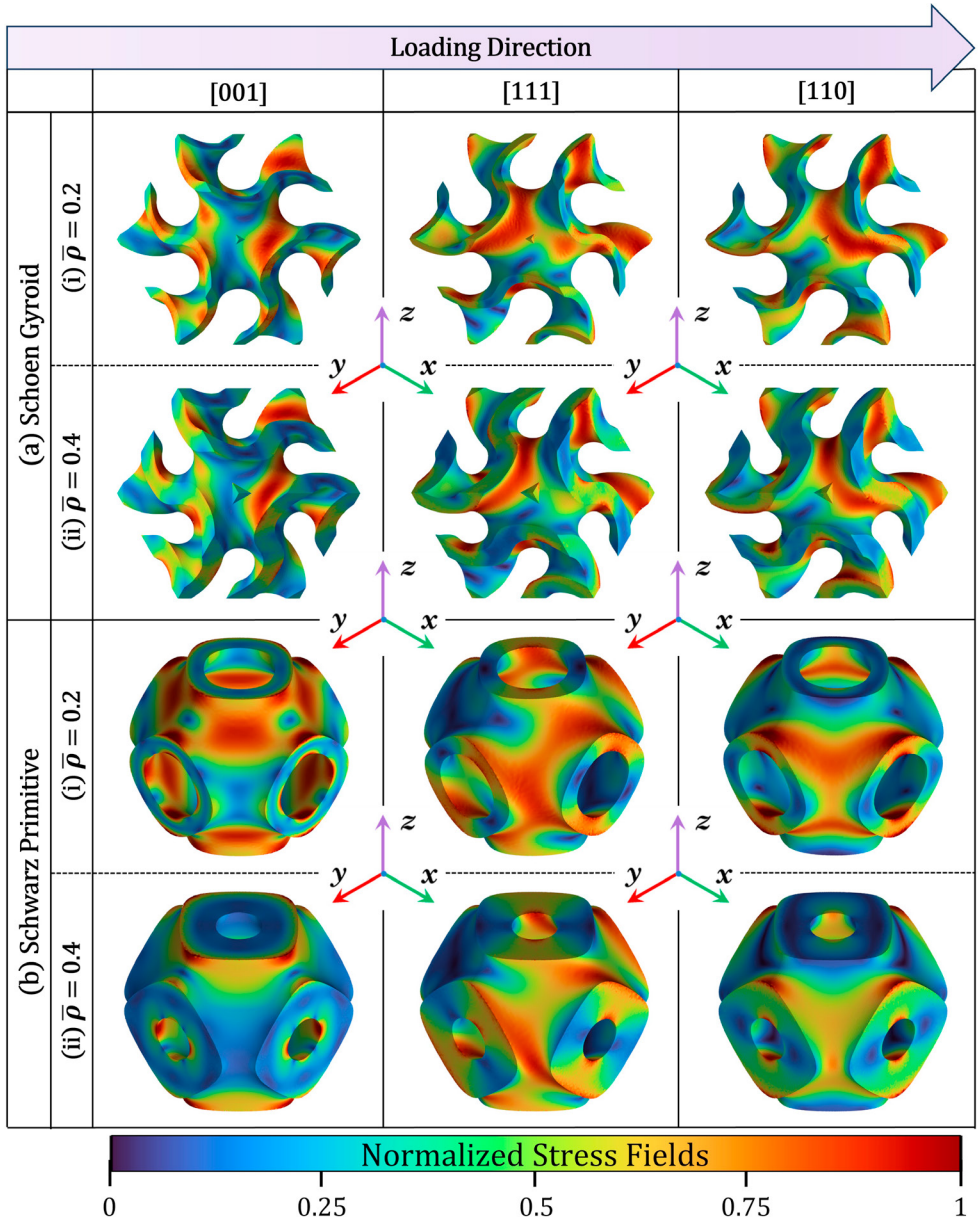


Fig. 5: Normalized stress field distribution referred to as Crossland FIP distribution for (a) Schoen Gyroid and (b) Schwarz Primitive.

## References

Abueidda, D.W., Abu Al-Rub, R.K., Dalaq, A.S., Lee, D.W., Khan, K.A., Jasiuk, I., 2016. Effective conductivities and elastic moduli of novel foams with triply periodic minimal surfaces. Mech. Mater. 95, 102-115.

Ahmadi, S., Yavari, S., Wauthle, R., Pouran, B., Schrooten, J., Weinans, H., Zadpoor, A., 2015. Additively manufactured open-cell porous biomaterials made from six different space-filling unit cells: The Mechanical and Morphological Properties. Materials 8(4), 1871–1896.

Al-Ketan, O., Abu Al-Rub, R.K., 2019. Multifunctional mechanical-metamaterials based on triply periodic minimal surface lattices. Adv. Eng. Mater. 21, 1900524.

Baghous, N., Barsoum, I., Abu Al-Rub, R.K., 2022. The effect of Lode parameter on the yield surface of Schoen's IWP triply periodic minimal surface lattice. Mech. Mater. 175, 104473.

Bobbert, F.S.L., Lietaert, K., Eftekhari, A.A., Pouran, B., Ahmadi, S.M., Weinans, H., Zadpoor, A.A., 2017. Additively Manufactured Metallic

Porous Biomaterials Based on Minimal Surfaces: A Unique Combination of Topological, Mechanical, and Mass Transport Properties. Acta Biomater. 53, 572-584.

Chatzigeorgiou, C., Boris, P., Yves, C., Pascal, L., and Fodil, M., 2022. Numerical Investigation of the Effective Mechanical Properties and Local Stress Distributions of TPMS-Based and Strut-Based Lattices for Biomedical Applications. J. Mech. Behav. Biomed. Mater. 126, 105025.

Crossland, B., 1956. Effect of large hydrostatic pressures on the torsional fatigue strength of an alloy steel. In: Proc. of Int. Conf. on Fatigue of Metals. London: IMechE, pp. 138-149.

Cutolo, A., Engelen, B., Desmet, W., Hooreweder, B.V., 2020. Mechanical properties of diamond lattice Ti–6Al–4V structures produced by laser powder bed fusion: On the effect of the load direction. J. Mech. Behav. Biomed. Mater. 104, 103656.

Downing, D., Jones, A., Brandt, M., and Leary, M., 2021. Increased Efficiency Gyroid Structures by Tailored Material Distribution." Mater. Des. 197, 109096.

Hill, R. 1963. Elastic properties of reinforced solids: Some Theoretical Principles. J. Mech. Phys. Solids, 11, 357-372.

Krishnan K., Lee, D.W., Teneji M.Al, Abu Al-Rub, R.K., 2022. Effective stiffness, strength, buckling and anisotropy of foams based on nine unique triple periodic minimal surfaces. Int. J. Solids Struct. 1, 111418.

Kelly, C.N., Evans, N.T., Irvin, C.W., Chapman, S.C., Gall, K., Safranski, D.L., 2019. The Effect of Surface Topography and Porosity on the Tensile Fatigue of 3D Printed Ti-6Al-4V Fabricated by Selective Laser Melting. Mater. Sci. Eng.: C 98, 726-736.

Lu, C., Mengting, H., Zhifeng, H., Chi, Z., Yaojun, L., Qiang, S., Fei, C., and Lianmeng Z., 2022. Architectural Design and Additive Manufacturing of Mechanical Metamaterials: A Review. Engineering 17, 44-63.

Maconachie, T., Leary, M., Lozanovski, B., Zhang, X., Qian, M., Faruque, O., Brandt, M.,2019. SLM lattice structures: Properties, performance, applications and challenges. Mater. Des. 183, 108137.

Maskery, I., A.O. Aremu, M. Simonelli, C. Tuck, R.D. Wildman, I.A. Ashcroft, and R.J.M. Hague, 2015. Mechanical Properties of Ti-6Al-4V Selectively Laser Melted Parts with Body-Centred-Cubic Lattices of Varying Cell Size. Exp. Mech. 55, 1261-1272.

Molavitabrizi, D., Ekberg, A., Mousavi, S.M., 2022. Computational model for low cycle fatigue analysis of lattice materials: Incorporating theory of critical distance with elastoplastic homogenization. Eur. J. Mech. A. Solids 92, 104480.

Nordmann, J., Aßmus, M., Altenbach, H., 2018. Visualising elastic anisotropy: theoretical background and computational implementation. Continuum Mech. Thermodyn. 30, 689-708.

Peng, X., Qiyuan Huang, Yali Zhang, Xiaogang Zhang, Tongtong Shen, Haoyu Shu, and Zhongmin Jin, 2021. Elastic Response of Anisotropic Gyroid Cellular Structures under Compression: Parametric Analysis. Mater. Des. 205, 109706.

Peng, Z., Zhang, D.Z., and Zhong, B., 2022. Constitutive and Damage Modelling of Selective Laser Melted Ti-6Al-4V Lattice Structure Subjected to Low Cycle Fatigue. Int. J. Fatigue 159, 106800.

Poltue, T., Karuna, C., Khrueaduangkham, S., Seehanam, S., Promoppatum, P., 2021. Design exploration of 3D-printed triply periodic minimal surface scaffolds for bone implants. Int. J. Mech. Sci. 211, 106762.

Refai, K., Brugger, C., Montemurro, M., Saintier, N., 2020. An Experimental and Numerical Study of the High Cycle Multiaxial Fatigue Strength of Titanium Lattice Structures Produced by Selective Laser Melting (SLM). Int. J. Fatigue 138, 105623.

Refai, K., Montemurro, M., Brugger, C., Saintier, N., 2020. Determination of the effective elastic properties of titanium lattice structures. Mech. Adv. Mater. Struct. 27, 1966-1982.

Sharma, D., Hiremath, S.S., 2020. Additively manufactured mechanical metamaterials based on triply periodic minimal surfaces: Performance, challenges, and application. Mech. Adv. Mater. Struct. 29, 5077-5107.

Vayssette, B., Saintier, N., Brugger, C., May, M. El., Pessard, E., 2019. "Numerical Modelling of Surface Roughness Effect on the Fatigue Behavior of Ti-6Al-4V Obtained by Additive Manufacturing." Int. J. Fatigue 123, 180-95.

Yavari, S.A., Ahmadi, S.M., Wauthle, R., Pouran, B., Schrooten, J., Weinans, H., and Zadpoor, A.A., 2015. Relationship between Unit Cell Type and Porosity and the Fatigue Behavior of Selective Laser Melted Meta-Biomaterials. J. Mech. Behav. Biomed. Mater. 43, 91-100.

Yang, L., Yan, C., Fan, H., Li, Z., Cai, C., Chen, P., Shi, Y., Yang, S., 2019. Investigation on the Orientation Dependence of Elastic Response in Gyroid Cellular Structures. J. Mech. Behav. Biomed. Mater. 90, 73-85.

Yang, L., Yan, C., Cao, W., Liu, Z., Song, B., Wen, S., Zhang, C., Shi, Y., Yang, S., 2019. Compression–Compression Fatigue Behaviour of Gyroid-Type Triply Periodic Minimal Surface Porous Structures Fabricated by Selective Laser Melting. Acta Mater. 18, 49-66.

Yu, X., Ji, Z., Haiyi, L., Zhengyi, J., Lingling, Wu., 2018. Mechanical Metamaterials Associated with Stiffness, Rigidity and Compressibility: A Brief Review. Prog. Mater Sci. 94, 114-73.

Zener, C.M., Siegel, S., 1949. Elasticity and Anelasticity of Metals. J. Phys. Chem. 53 (9).